

Magnetism in $\text{Sr}_2\text{CrMoO}_6$: A Combined Ab-initio and Model Study

Prabuddha Sanyal¹, Anita Halder², Liang Si³, Markus Wallerberger³, Karsten Held³ and Tanusri Saha-Dasgupta²

¹ *Department of Physics, Indian Institute of Technology, Roorkee 247667, India*

² *Department of Condensed Matter Physics and Materials Science, S.N. Bose National Center for Basic Sciences, Kolkata, India and*

³ *Institute for Solid State Physics, TU Wien, 1040 Wien, Austria*

(Dated: November 5, 2018)

Using a combination of first-principles density functional theory (DFT) calculations and exact diagonalization studies of a first-principles derived model, we carry out a microscopic analysis of the magnetic properties of the half-metallic double perovskite compound, $\text{Sr}_2\text{CrMoO}_6$, a sister compound of the much discussed material $\text{Sr}_2\text{FeMoO}_6$. The electronic structure of $\text{Sr}_2\text{CrMoO}_6$, though appears similar to $\text{Sr}_2\text{FeMoO}_6$ at first glance, shows non trivial differences with that of $\text{Sr}_2\text{FeMoO}_6$ on closer examination. In this context, our study highlights the importance of charge transfer energy between the two transition metal sites. The change in charge transfer energy due to shift of Cr d states in $\text{Sr}_2\text{CrMoO}_6$ compared to Fe d in $\text{Sr}_2\text{FeMoO}_6$ suppresses the hybridization between Cr t_{2g} and Mo t_{2g} . This strongly weakens the hybridization-driven mechanism of magnetism discussed for $\text{Sr}_2\text{FeMoO}_6$. Our study reveals that, nonetheless, the magnetic transition temperature of $\text{Sr}_2\text{CrMoO}_6$ remains high since additional superexchange contribution to magnetism arises with a finite intrinsic moment developed at the Mo site. We further discuss the situation in comparison to another related double perovskite compound, Sr_2CrWO_6 . We also examine the effect of correlation beyond DFT, using dynamical mean field theory (DMFT).

PACS numbers: 71.20.-b, 71.20.Be, 75.50.-y

I. INTRODUCTION

In recent years, double perovskites with general formula $\text{A}_2\text{BB}'\text{O}_6$ (A: rare-earth/alkaline-earth cation, B: $3d$ transition metal, B': $4d/5d$ transition metal) have been in focus of discussion due to their attractive properties. This includes multiferrocity,^{1,2} magnetodielectric and magnetocapacitive properties,^{3,4} complex spin behavior,⁵ magneto-structural coupling⁶ etc. Many of these compounds show half-metallic behavior, which is of importance for spintronics and related technological applications.⁷⁻¹⁴ The high magnetic transition temperatures (T_c) exhibited by compounds like $\text{Sr}_2\text{FeMoO}_6$, open up the possibility of room temperature application.^{15,16} The pioneering work, reporting¹⁵ room temperature magnetoresistivity of $\text{Sr}_2\text{FeMoO}_6$ (SFMO) was met with excitement and followed by a surge of activity exploring the dependence of $3d$ transition metal (TM) ion on the properties of these compounds.

Following this motivation, Cr-based double perovskites have been synthesized and studied,¹⁷ in particular, the sister compound of SFMO, $\text{Sr}_2\text{CrMoO}_6$ (SCMO).¹⁸ Unlike in SFMO, there can be no valence compensation between Cr and the Mo in SCMO: Cr can only be in the $3+$ state making $\text{Cr}^{3+}/\text{Mo}^{5+}$ only possible combination, while for SFMO, both $\text{Fe}^{3+}/\text{Mo}^{5+}$ and $\text{Fe}^{2+}/\text{Mo}^{6+}$ combinations are possible. Thus, SCMO was expected to be an even better candidate for room temperature spintronics. However, although the measured transition temperature of SCMO is high,^{18,19} the observed moment²⁰ and the magnitude of the tunneling magnetoresistance turned to be disappointingly low. The presence of large antisite disorder, together with oxygen vacancy was held

responsible for this.¹⁹ The antisite disorder present in the samples was estimated to be as high as 43 - 50 %.^{18,21} To appreciate the role of $3d$ TM in the properties of double perovskites, it is thus highly desirable to understand the electronic and magnetic properties of pure SCMO.

Theoretical studies on SCMO have been carried out within the framework of DFT.^{22,23} However no microscopic analysis has been carried out, neither has the transition temperature been calculated, except for a recent mean field analysis²⁴ based on a classical Ising model. The latter neglects the itinerant electronic character of Mo $4d$ electrons, a crucial component in understanding the behavior of these $3d$ - $4d$ double perovskites.

Futhermore, though the hybridization driven mechanism of magnetism has been identified¹⁰ a while ago as the driving force in setting up the high Curie temperature in compounds like SFMO, the role of charge transfer between B and B' sites in the perspective of properties of double perovskite compounds in general, has not been studied in detail. In particular no systematic study exists. This is however an important issue in understanding the comparative magnetic properties of double perovskite compounds.

In the present study, we aim to fill this gap by combining state-of-art DFT calculations and exact diagonalization of the DFT derived model Hamiltonian. We consider the case of SCMO, in comparison to SFMO as well as Sr_2CrWO_6 (SCWO)¹⁷ which is another double perovskite from the Cr family but with $5d$ W instead of $4d$ Mo. Our microscopic study shows a considerable suppression of the Cr t_{2g} - Mo t_{2g} hybridization in SCMO compared to that in SFMO or SCWO, driven by the change in charge transfer energy between B and B' sites in different compounds. The suppressed hybridization in

SCMO makes the Mo t_{2g} electrons more localized compared to SFMO or SCWO. This, in turn, opens up an additional, super-exchange contribution to magnetism. The calculated magnetic transition temperature T_c without super-exchange contribution, gives about 79 % of the measured T_c . The consideration of additional super-exchange contribution makes the calculated T_c comparable to the measured one. Our work reveals the importance of the super-exchange in SCMO in addition to the hybridization-driven mechanism operative in SFMO or SCWO, and underlines the crucial role played by the charge transfer energy in activating the additional superexchange channel in SCMO.¹⁵

We further study the effect of correlation on the half-metallic property of SCMO by including local correlations on top of DFT within the framework of DMFT. The DMFT results confirm the half-metallic ground state below the magnetic transition temperature, implying that the qualitative description remains unaffected by correlation effects.

II. COMPUTATIONAL DETAILS

The first-principles DFT calculations have been carried out using the plane-wave pseudopotential method implemented within the Vienna Ab-initio Simulation Package (VASP).²⁵ The exchange-correlation functional was considered within the generalized gradient approximation (GGA) in the framework of PW91.²⁶ Additionally calculations have been carried with exchange-correlation functional of local density approximation (LDA)²⁷ as well as GGA within the framework of PBE,²⁸ in order to check any possible influence of the exchange-correlation functional on the calculated electronic structure. The projector-augmented wave (PAW) potentials²⁹ were used and the wave functions were expanded in the plane-wave basis with a kinetic-energy cutoff of 500 eV. Reciprocal-space integrations were carried out with a k -space mesh of $8 \times 8 \times 8$.

In order to extract a few-band tight-binding (TB) Hamiltonian out of the full DFT calculation which can be used as input to multiorbital, low-energy model Hamiltonian in exact diagonalization calculations we have carried out N -th order muffin tin orbital (NMTO) calculations.³⁰ A prominent feature of this method is the downfolding scheme. Starting from a full DFT calculation, it defines a few-orbital Hamiltonian in an energy-selected, effective Wannier function basis, by integrating out the degrees of freedom that are not of interest. The NMTO technique relies on the self-consistent potential parameters obtained out of linear muffin-tin orbital (LMTO)³¹ calculations. In order to cross-check the TB parameters generated out of NMTO-downfolding calculations, further calculations were carried out using wien2wannier³². This generates maximally localized Wannier functions³³ from Wien2K³⁴ which employs a full potential linear augmented plane wave (FLAPW) basis.

For self-consistent DFT calculation in the FLAPW basis the number of k -points in the irreducible Brillouin zone was chosen to be 64. The commonly used criterion relating the plane wave and angular momentum cutoff, $l_{max} = R_{MT} \times K_{max}$ was chosen to be 7.0, where R_{MT} is the smallest MT sphere radius and K_{max} is the plane wave cutoff for the basis. The chosen atomic radii for Sr, Cr, Mo and O were 1.43 Å, 1.01 Å, 1.01 Å, and 0.87 Å, respectively.

The exact diagonalization of the ab-initio derived low-energy Hamiltonian, defined in the Wannier function basis has been carried out for finite-size lattices of dimensions $4 \times 4 \times 4$, $6 \times 6 \times 6$, and $8 \times 8 \times 8$. The results presented in the following are for $8 \times 8 \times 8$ lattice.

The DFT+DMFT calculations^{35,36} have been carried out using the wien2wannier³²-derived maximally localized Wannier functions of Wien2K as a starting point. We restricted the DMFT to the low energy degrees of freedom, i.e., to the “ t_{2g} ” orbitals of Mo and the “ t_{2g} ” and “ e_g ” orbitals of Cr (These low energy orbitals are actually a mixture between predominately transition metal t_{2g} (e_g) character with some admixture of oxygen p character). We supplemented the DFT low-energy Hamiltonian in the Wannier basis by a local Coulomb interaction in Kanamori parametrization. For details see Ref. 37. For the interaction values we chose the typical values for $3d$ and $4d$ transition metal oxides. The choices were: interorbital Coulomb repulsion of $U' = 4$ eV (2.4 eV) and a Hund’s coupling $J_H = 0.7$ eV (0.3 eV) for Cr (Mo) as estimated for neighboring vanadium³⁸(ruthenium³⁹) perovskites. The intraorbital (Hubbard) repulsion follows from orbital symmetry as $U = U' + 2J_H$; and the pair hopping term is of equal strength as J_H . As a DMFT impurity solver, continuous-time quantum Monte-Carlo simulations⁴⁰ in the w2dynamics³⁷ implementation was used which includes the full SU(2) symmetry. The effect of electronic correlations beyond GGA, within the framework of static theory was also checked by performing GGA+ U calculations with choice of same U parameters, as in DMFT calculation. We have also checked the validity of our results by varying the U value by ± 1 eV at Cr site, and by ± 0.5 eV at Mo site. The trend in the results was found to remain unchanged.

III. RESULTS

A. Basic DFT Electronic Structure

We first revisit the basic DFT electronic structure of SCMO, which has been calculated before using variety of basis sets, including plane wave,⁴¹ LAPW²² and LMTO.²³ SCMO crystallizes in the cubic Fm3m space group (225), with lattice parameter of 7.84 Å.¹⁹

The upper panel of Fig 1. shows the spin polarized density of states (DOS) calculated in a plane wave basis. The basic features of the DOS, which agree very well with previous studies^{22,23,41} are the following: The states

close to Fermi level, E_F , (set as zero in the figure), are dominated by Cr and Mo d states hybridized with O p states. The states of dominant O p character are positioned further down in energy, separated by a small gap from Cr and Mo d states. Empty Sr states, not shown in the energy scale of the figure, remain far above E_F . Due to the large octahedral crystal field at Mo sites, the empty Mo e_g states lie far above E_F . The Cr t_{2g} states are occupied in the up spin channel and empty in the down spin channel. Cr e_g states are empty in both spin channels, in agreement with the nominal Cr^{3+} (d^3) valence. The empty and highly peaked Mo t_{2g} states in the up spin channel appear in between the crystal field split Cr t_{2g} and Cr e_g states for the same spin. In contrast for the down spin channel, the Mo t_{2g} hybridize more strongly with Cr t_{2g} , which explains their much larger bandwidth.

The above described basic features for B and B' states, are rather similar for SCMO and SFMO,⁴² and in that respect also for SCWO.⁴³ Nevertheless, the DOS of SCMO differs from both SFMO and SCWO in important details. The hybridization between B t_{2g} and B' t_{2g} in the down spin channel, is found to be significantly lower compared to that of SFMO or SCWO.^{42,43} A measure of this is the Cr contribution in the down spin bands crossing E_F of predominant Mo character. We estimate this contribution or admixture to be 35% for SCMO, while the corresponding estimates for SCWO and SFMO are much larger, 66% and 72 %, respectively.

The top rows in Table I show the calculated magnetic moments at Cr and Mo sites, as well as the total moment in three choices of exchange-correlation functionals, GGA-PW91, GGA-PBE as well as LDA. The half-metallic nature of the ground state is found to be robust in all different choices of exchange-correlation functionals with the total magnetic moment of $2.0 \mu_B/\text{f.u.}$ and finite moments residing at O sites. As is seen, while the individual moments on Cr and Mo are found to vary depending on the nature of approximation, the magnetic moments on Cr and Mo site being aligned in an antiparallel manner, the enhancement/reduction of individual moments cancel, thereby retaining the half-metallicity and net moment of $2 \mu_B/\text{f.u.}$ Our calculated GGA magnetic moments at Cr and Mo sites are in good agreement with that reported by Liet *et al.*⁴¹ The calculated site-specific moment reported by Wu²³ is however much smaller than that of our as well as that of Liet *et al.*⁴¹ This is presumably due to different choices of the muffin tin radii as well as the exchange-correlation functional.

The measured magnetic moments are significantly smaller than the theoretical values. Experimentally, the total moment is only $0.5 \mu_B$ ²⁰ and the moment on the Cr sites is $0.8 \mu_B$.⁴⁴ This discrepancy was hitherto argued to be due to the large disorder present in the sample.¹⁹ It is interesting to note that the value of the calculated GGA-PW91 magnetic moment at the Mo sites ($0.43 \mu_B$) is larger than the calculated B' site moment for SFMO ($0.23 \mu_B$) and SCWO ($0.30 \mu_B$). This indicates a weaker

	Sr	Cr	Mo	total
LDA	0.00	-2.18	0.32	-2.00
GGA-PW91	0.00	-2.29	0.43	-2.00
GGA-PBE	0.00	-2.36	0.49	-2.00
GGA+ U	0.00	-2.54	0.58	-2.00
DMFT	0.00	-2.84	0.84	-2.00

Table I: Calculated magnetic moments (in μ_B) within LDA, GGA-PW91, GGA-PBE, GGA+ U and DMFT. Note that within GGA there is also a moment on the oxygen sites which is accounted for in the Cr and Mo moment in DMFT as the predominately metal d Wannier functions also have some oxygen admixture.

itinerancy of the Mo electrons in SCMO, compared to SFMO or to that of W in SCWO. This in turn suggests that a small, but finite intrinsic moment develops at the Mo site as a consequence of the weaker hybridization between Cr and Mo. The suppression of the hybridization and the reduced itinerancy of the Mo t_{2g} electrons in SCMO has been also pointed out in the study by Wu,²³ though no detailed understanding of the mechanism of magnetism was provided. In the following we will elaborate on the microscopic mechanism of magnetism in SCMO.

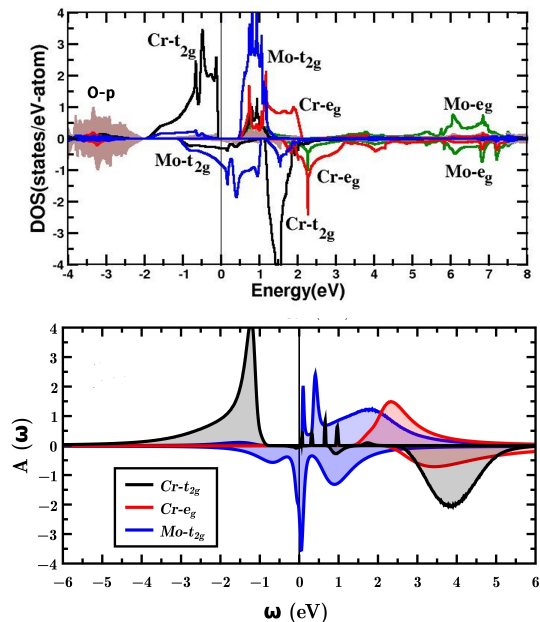


Figure 1: (Color online) Upper panel: GGA-PW91 spin-polarized DOS projected onto Cr t_{2g} (black solid line), Cr e_g (red solid line), Mo t_{2g} (blue solid line), Mo e_g (green solid line) and O p (shaded area) in the FLAPW basis. The zero of the energy is set to the Fermi energy. The positive (negative) axis of DOS corresponds to DOS in up (down) spin channel. Lower panel: DMFT spectral density, calculated at 200 K within the Mo t_{2g} and Cr $t_{2g} + e_g$ Wannier basis.⁴⁵

B. DMFT Spectral Density

In order to study the effect of electronic correlations, specially the dynamical correlation which may be important for SCMO due to the metallic nature of the ground state, we further carry out DMFT calculations in the Wannier function basis. The lower panel in Fig 1, shows the DMFT spectral density calculated at a temperature of 200 K.

The spectrum shows qualitatively similar behavior to that obtained in DFT calculation, though the down spin spectrum shows the correlation physics with a feature resembling lower and upper Hubbard bands and a well defined quasi-particle peak at Fermi energy. This demonstrates the dual nature of the Mo down spin with localized electrons (Hubbard bands) and itinerant electrons (quasiparticle band) at the same time. The fully spin-polarized conducting electrons are Fermi-liquid-like with a linear frequency-dependence of the self energy (not shown). Hence the quasiparticle peak will lead to a Drude peak in the optical conductivity.

The DMFT magnetic moments are shown in the last row of Table I. We note the DMFT calculated magnetic moments are in the basis of Cr and Mo t_{2g} Wannier functions, which includes the effect of oxygen. This makes a direct comparison between DMFT and GGA values somewhat more difficult. However since the difference between GGA and DMFT magnetic moments is larger than the GGA oxygen contribution, we can conclude that electronic correlations somewhat enhance the magnetic moment on both, Mo and Cr, sites. This is further supported by the magnetic moments calculated within the static theory of GGA+ U , with choice of same U parameters as in DMFT calculation, shown in the second row of Table I, which shows an enhancement of the moment both at Cr and Mo sites, compared to that of GGA.

C. Few-orbital, low-energy Hamiltonian

In order to understand the driving mechanism of magnetism in SCMO in a more quantitative manner, we carry out a NMTO downfolding in order to estimate the positions of exchange split Mo t_{2g} energy levels, before and after switching on the hybridization between the Mo t_{2g} and Cr t_{2g} . The former provides the estimate of intrinsic spin splitting at the Mo site, while the latter provides the information of the spin splitting at the Mo site renormalized by the hybridization effect from Cr t_{2g} . As a first step of this procedure, we downfold O p , Sr as well as Cr and Mo e_g degrees of freedom. This defines a few-orbital Hamiltonian consisting of Cr t_{2g} and Mo t_{2g} states. In the second step, we perform a further downfolding, keeping only the Mo t_{2g} degrees of freedom, i.e., downfolding everything else including the Cr t_{2g} degrees of freedom. On site matrix elements of the few orbital Hamiltonian in real space representation defined in the Cr t_{2g} - Mo t_{2g} basis and the massively downfolded basis give the energy

level positions before and after switching of the hybridization, respectively. The obtained result is presented in Fig 2. First of all, we notice that the Mo t_{2g} states are energetically situated in between the exchange-split energy levels of Cr t_{2g} 's. Thus switching of the hybridization between Cr and Mo, pushes the Mo up spin states down because these are below the Cr states of the same spin. In contrast, the Mo down spins are above their Cr counterpart and hence the hybridization shifts them upwards. Thus the hybridization induces a renormalization of the spin splitting at the Mo site, with renormalized value of about 0.70 eV, and being oppositely oriented (negative) with respect to that at Cr site. Note the intrinsic (in absence of hybridization) spin splitting at Mo site is small, having a value of 0.15 eV.

In this respect, the situation is very similar to SFMO or SCWO, for which also a negative splitting is induced at the itinerant B' sites because of the hybridization with the large spin at the B sites.^{10,15,43,46} This supports that the hybridization-driven mechanism is operative in SCMO as well. While in all three cases of SFMO, SCWO and SCMO, the B' t_{2g} states appear in between the strong exchange split energy levels of B site, which is an essential ingredient for hybridization-driven mechanism to be operative, we notice the relative energy position of B' t_{2g} states with respect to the exchange split B states is different in case of SCMO, as compared to SFMO or SCWO. For SFMO or SCWO, the down spin B' t_{2g} states appear very close to B site down spin states, while for SCMO, they are shifted down.^{15,43} This hints towards a significantly different charge transfer energy in case of SCMO as compared to SFMO or SCWO. This will be elaborated in the next paragraphs. We further notice that the intrinsic splitting at the Mo sites (0.15 eV) is somewhat larger than for SCWO (0.05 eV).⁴³ This further confirms the conclusion drawn from the calculated magnetic moment at Mo site that is in SCMO, unlike SFMO, Mo has a finite intrinsic moment. The magnetism in SCMO, as mentioned already, thus has an additional contribution, originating from the superexchange between the large moment at the Cr site and the intrinsic moment at the Mo site, on top of the hybridization-driven mechanism, as operative in SFMO. Note that the superexchange is antiferromagnetic, aligning the Cr and Mo moments antiparallely, *i.e.*, in the same way as for the hybridization-driven mechanism.

In this situation, the low-energy model Hamiltonian for SCMO in the Cr t_{2g} and Mo t_{2g} Wannier basis, describing the hybridization and super-exchange mechanism is given

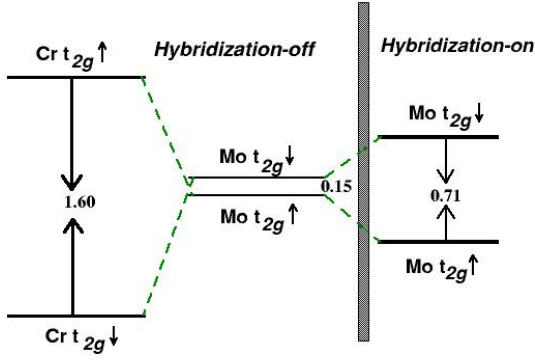


Figure 2: (Color online) The energy level diagram for SCMO, in the absence and presence of the Cr-Mo hybridization. The energies are in units of eV.

by^{43,47}

$$\begin{aligned}
 H = & \epsilon_{Cr} \sum_{i \in B} f_{i\sigma\alpha}^\dagger f_{i\sigma\alpha} + \epsilon_{Mo} \sum_{i \in B'} m_{i\sigma\alpha}^\dagger m_{i\sigma\alpha} \\
 & - t_{Cr-Mo} \sum_{\langle ij \rangle, \sigma, \alpha} f_{i\sigma, \alpha}^\dagger m_{j\sigma, \alpha} \\
 & - t_{Mo-Mo} \sum_{\langle ij \rangle, \sigma, \alpha} m_{i\sigma, \alpha}^\dagger m_{j\sigma, \alpha} \\
 & - t_{Cr-Cr} \sum_{\langle ij \rangle, \sigma, \alpha} f_{i\sigma, \alpha}^\dagger f_{j\sigma, \alpha} + J \sum_{i \in Cr} \mathbf{S}_i \cdot f_{i\alpha}^\dagger \vec{\sigma}_{\alpha\beta} f_{i\beta} \\
 & + J' \sum_{i \in Cr, j \in Mo} \mathbf{S}_i \cdot \mathbf{s}_j. \quad (1)
 \end{aligned}$$

Here the f 's and m 's are second quantization operators for the Cr t_{2g} and Mo t_{2g} degrees of freedoms; σ is the spin index and α is the orbital index that spans the t_{2g} manifold; t_{Cr-Mo} , t_{Mo-Mo} , t_{Cr-Cr} represent the nearest neighbor Cr-Mo, the second nearest neighbor Mo-Mo and the Cr-Cr hopping, respectively. The on-site energy difference between Cr t_{2g} and Mo t_{2g} levels is $\Delta = \epsilon_{Cr} - \epsilon_{Mo}$. To take into account the dual nature of the electrons that are both, itinerant and localized, we include a large core spin \mathbf{S}_i at the Cr site that couples with the itinerant electron delocalized over the Cr-Mo network, via a double-exchange like mechanism. The last term represents the superexchange mechanism in terms of coupling between the Cr spin (\mathbf{S}_i) and the intrinsic moment on the Mo site (\mathbf{s}_j).

All TB parameters of the model Hamiltonian, i.e., Δ , t_{Cr-Mo} , t_{Mo-Mo} , t_{Cr-Cr} , are extracted from a non-spin-polarized DFT calculations through two independent means: a) through the NMTO downfolding technique, and b) through the construction of maximally localized Wannier functions in the basis of the effective Cr and Mo t_{2g} degrees of freedom. The latter scheme has been also employed in the DMFT study, presented before. In both cases we integrate out all other degrees of freedom except for the Cr and Mo t_{2g} 's states. The comparison of the full DFT non spin-polarized band structure and the few orbital TB bands in maximally localized

	Δ	t_{Cr-Mo}	t_{Mo-Mo}	t_{Cr-Cr}
SCMO (NMTO)	-0.35	0.33	0.14	0.08
SCMO (Wannier90)	-0.42	0.30	0.12	0.06
SCWO	-0.66	0.35	0.12	0.08
SFMO	-1.04	0.26	0.11	0.04

Table II: Tight-binding parameters (in eV) of the few orbital Hamiltonian for SCMO, SCWO⁴³, and SFMO⁴² in Wannier function basis, extracted out of DFT calculations.

Wannier function basis is shown in Fig 3. The agreement between the two is found to be as good as possible, proving the effectiveness of the Wannier function projection.

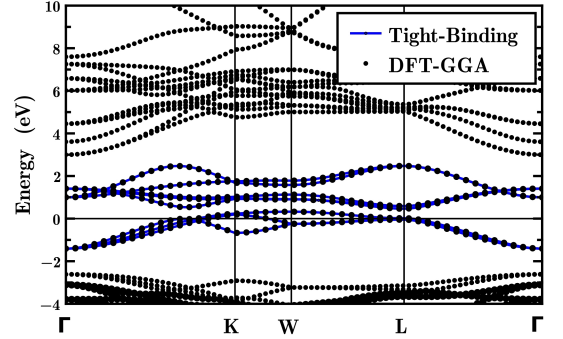


Figure 3: (Color online) Comparison of the full paramagnetic DFT band structure (solid line) and the few orbital TB band structure (+) plotted along a high symmetry path through the Brillouin zone [Γ : (0 0 0), K: (3/8, 3/4, 3/8), W: (1/4, 3/4, 1/2), L: (1/2, 1/2, 1/2) and X: (0, 1/2, 1/2)].

The DFT estimates of Δ , t_{Cr-Mo} , t_{Cr-Cr} and t_{Mo-Mo} , obtained by two different scheme of calculations are shown in Table II. The agreement of the values in two independent scheme of calculations is remarkable and provides confidence regarding the results. The TB parameters for SCWO⁴³ and SFMO⁴² are also listed in the table for comparison.

While the estimated hopping parameters of SCMO are rather similar to that reported for SCWO,⁴³ we find the charge transfer energy Δ (-0.4 eV) to be quite different from that estimated for SFMO (-1.0 eV)⁴² and for SCWO (-0.7 eV).⁴³ This forms the most crucial observation of our study, which dictates the differences in electronic structure of SCMO and, SFMO and SCWO. Related discussions involving importance of Δ and t in hybridization driven mechanism were mentioned by another group for comparisons between SFMO and A-site B-site randomly doped Ti oxides although it was not a systematic one.⁴⁸

The change in the bare, non-spin-polarized charge transfer energy (Δ), in turn, modifies the renormalized charge transfer energy Δ_R between Cr and Mo in the down spin channel in the spin-polarized phase. It is much larger in SCMO (0.81 eV) compared to that in SCWO (0.51 eV),⁴³ due to the moving down the column of the periodic table from the 4d element Mo in SCMO to the

5d element W in SCWO. As a consequence of the larger charge transfer splitting Δ_R the effect of the hybridization which is governed by t_{C-Mo}^2/Δ_R is significantly suppressed in SCMO, by about 63% compared to the corresponding value for SCWO.

The parameter involving J in (1) corresponds to the spin-splitting at the Cr site, while J' is obtained from the enhanced intrinsic spin-splitting observed at Mo site in case of SCMO as compared to that for SCWO compound at the W site. As discussed below, frustration effects make the convergence of total energy calculations in different spin configurations difficult, prohibiting direct extraction of J' in a single system. Thus J' needs to be determined by comparison of the independently obtained intrinsic spin splittings (obtained by turning off the B-B' hybridization) at the B' sites of the related compounds. This approach was used earlier,⁴³ where three compounds Sr_2CrWO_6 , Sr_2CrReO_6 and Sr_2CrOsO_6 were considered. It was pointed out⁴³ that the intrinsic splitting at the B site due to a purely hybridization driven mechanism should increase proportional to the electron filling at B' site (the filling increases from 1 to 2 to 3 moving from W to Re to Os); the additional increase, if any, is due to the presence of the localized moment at B' site giving rise to superexchange J' between B and B sites. In the present case, all the three compounds considered, namely SFMO, SCMO and SCWO have the same electron filling, namely 1. Hence considering the compound SCWO as the benchmark, the difference in intrinsic splitting between the Mo site of SCMO and the W site of SCWO is used to obtain the J' value for SCMO.⁴⁹

D. Exact Diagonalization of Model Hamiltonian

As the magnetism of SCMO turns out to be driven by both hybridization-driven mechanism and superexchange mechanism, the calculation of magnetic transition temperature in a first-principles way is challenging. For example, an antiferromagnetic configuration of Cr spins leads to a frustration of the intrinsic Mo moment. On the other hand, the hybridization-driven mechanism, disfavors the stabilization of magnetic configurations with Cr spins aligned in parallel to the spins at Mo sites. This thus leads to a frustration effect which makes the convergence of different spin configurations to extract the magnetic exchanges a challenge within the framework of full blown DFT scheme.

Hence, we consider the model Hamiltonian approach in the following. To this end, we solve the ab-initio constructed model Hamiltonian (1) using exact diagonalization on a finite lattice. In particular, we consider the stability of the ferromagnetic arrangements of Cr spins measured as the energy difference between the paramagnetic (PM) spin configuration and the ferromagnetic (FM) spin configuration. The PM phase was simulated as disordered local moment calculations, where the calculations were carried out for several (≈ 50) disordered

configurations of Cr spin and were averaged to get the energy corresponding to PM phase. This energy difference provides an estimate of the magnetic T_c .

In order to check the influence of the intrinsic moment at the Mo site on the magnetic transition, we first carried out exact diagonalization calculation considering the Mo site to be totally nonmagnetic, i.e., setting the last term of Hamiltonian (1) to zero. This boils down to a hybridization-only driven mechanism of magnetism, as suitable for SFMO or SCWO.^{43,50} The energy difference between the PM and FM in this calculation, turned out to be 0.067 eV/f.u., which is of the same order as, but less than, that obtained using the TB parameters of SCWO (0.085 eV/f.u.).^{43,51} As mentioned already, the hopping parameters between SCMO and SCWO are very similar, thus the difference is caused by the different charge transfer energy in the two compounds. Mapping this energy difference to the mean field transition temperature, one would get T_c in SCMO to be 79 % smaller compared to that of SCWO.¹⁷ The calculated PM and FM energy difference, considering the full model Hamiltonian, describing both hybridization-driven and super-exchange driven mechanism, is 0.080 eV/f.u., which makes the calculated T_c of SCMO similar to that of SCWO. Mapping the PM and FM energy difference to the mean field T_c , one obtains the values 822 K for SCMO and 870 K for SCWO, which are an overestimation of the experimental values.¹⁷⁻¹⁹ This is presumably due to non-local fluctuations beyond mean-field. However, the trend is very well reproduced with $T_c^{SCMO}/T_c^{SCWO} = 0.95$.

IV. SUMMARY

Starting from a DFT description we provide a microscopic analysis of the magnetic behavior of SCMO, a sister compound of SFMO. DFT calculations on pure, defect-free SCMO show that, like SFMO and SCMO, it is a half-metallic magnet. The calculated DMFT results confirm the robustness of the half-metallicity of SCMO upon inclusion of dynamical correlation effect. The DMFT results show a splitting of the Mo down spin band into Hubbard bands and quasiparticle peak. This indicates the dual nature of the Mo electrons having both, a local spin moment and itinerant behavior.

The origin of magnetism in SCMO turns out to be somewhat different than in SFMO. The charge transfer energy between Cr and Mo in the down spin channel of SCMO is found to be larger than that between Fe and Mo in SFMO. This suppresses the effect of hybridization between B and B' sites in SCMO compared to SFMO and has two consequences: (i) the hybridization-driven mechanism for magnetism is reduced and (ii) a small but finite intrinsic moment develops at the Mo sites. The latter gives rise to a partial localized character of the Mo electrons, which was absent in SFMO. This in turn opens up a super-exchange contribution to magnetism in SCMO, which was absent for SFMO. We compare our

results on SCMO to another Cr based double perovskite, SCWO. The magnetism in the latter, like SFMO, is well described by a hybridization-only picture. The computed T_c obtained through exact diagonalization of the ab-initio derived model Hamiltonian show the T_c of SCMO to be similarly high as in SCWO, only upon inclusion of both, super-exchange and hybridization-driven contribution in case of SCMO. Thus while magnetism in both, SCWO and SFMO, is governed by hybridization, the story in SCMO appears with a twist. It needs to be described by a combination of hybridization and superexchange mechanism.

We conclude that, in general, the magnetism in the double perovskite family has to be understood as an interplay between the hybridization and super-exchange between B and B' sites. The relative contribution of one mechanism vs. the other one is dictated by the charge transfer between the 3d transition metal at the B site

and the 4d or 5d transition metal at the B' site.

Acknowledgement

PS acknowledges the SRIC project No PHY/FIG/100625. AH and TSD acknowledge support from DST through thematic Unit of Excellence on Computational Materials Science; LS and KH from the European Research Council under the European Union's Seventh Framework Program (FP/2007-2013)/ERC through grant agreement n. 306447 and the Austrian Science Fund (FWF) through the Doctoral School W1243 Solids4Fun (Building Solids for Function). We are grateful to Tulika Moitra, P. Gunacker and D.D. Sarma for valuable discussions.

-
- ¹ Masaki Azuma, Kazuhide Takata, Takashi Saito, Shintaro Ishiwata, Yuichi Shimakawa, Mikio Takano, *J. Am. Chem. Soc.* **127**, 8889 (2005).
 - ² Vivien S. Zapf, B. G. Ueland, Mark Laver, Martin Lonsky, Merlin Pohlit, Jens Mller, Tom Lancaster, Johannes S. Mller, Stephen J. Blundell, John Singleton, Jorge Mira, Susana Yaez-Vilar, and Maria Antonia Sears-Rodrguez *Phys. Rev. B* **93**, 134431 (2016).
 - ³ Hena Das, Umesh V. Waghmare, T. Saha-Dasgupta, D. D. Sarma, *Phys. Rev. Lett.* **100**, 186402 (2008).
 - ⁴ Santu Baidya and T. Saha-Dasgupta *Phys. Rev. B* **84**, 035131 (2011).
 - ⁵ Sudipta Kanungo, Binghai Yan, Claudia Felser, and Martin Jansen, *Phys. Rev. B* **93**, 161116(R) (2016); Madhav Prasad Ghimire, Long-Hua Wu, and Xiao Hu, *Phys. Rev. B* **93**, 134421 (2016); S. M. Disseler, J. W. Lynn, R. F. Jardim, M. S. Torikachvili, and E. Granado, *Phys. Rev. B* **93**, 140407(R) (2016); Tomoyuki Koga, Nobuyuki Kurita, Maxim Avdeev, Sergey Danilkin, Taku J. Sato, and Hidekazu Tanaka, *Phys. Rev. B* **93**, 054426 (2016).
 - ⁶ Dexin Yang, Richard J. Harrison, Jason A. Schiemer, Giulio I. Lampronti, Xueyin Liu, Fenghua Zhang, Hao Ding, Yan'gai Liu, and Michael A. Carpenter, *Phys. Rev. B* **93**, 024101 (2016).
 - ⁷ T. Saitoh, M. Nakajima, A. Kakizaki, H. Nakajima, O. Morimoto, Sh. Xu, Y. Moritomo, N. Hamada, Y. Aiura, *Phys. Rev. B* **66**, 035112 (2002).
 - ⁸ T. Saitoh, M. Nakatake, H. Nakajima, O. Morimoto, A. Kakizaki, Sh. Xu, Y. Moritomo, N. Hamada, Y. Aiura, *Journal of Electron Spectroscopy and Related Phenomena* **144-147**, 601 (2005).
 - ⁹ Y. Tomioka, T. Okuda, Y. Okimoto, R. Kumai, K.-I. Kobayashi, Y. Tokura, *Phys. Rev. B* **61**, 422 (2000).
 - ¹⁰ D.D. Sarma, P. Mahadevan, T. Saha Dasgupta, S. Ray, A. Kumar, *Phys. Rev. Lett.*, **85**, 2549 (2000).
 - ¹¹ B Garca-Landa, C Ritter, MR Ibarra, J Blasco, PA Algarabel, R Mahendiran, J Garca, **110**, 435 (1999).
 - ¹² B. Martinez, J. Navarro, L. Balcells and J. Fontcuberta, *J. Phys.: Condens. Matter* **12**, 10515 (2000).
 - ¹³ D. D. Sarma, S. Ray, K. Tanaka, M. Kobayashi, A. Fujimori, P. Sanyal, H.R. Krishnamurthy and C. Dasgupta, *Phys. Rev. Lett.*, **98**, 157205 (2007).
 - ¹⁴ T. Saitoh, M. Nakajima, H. Nakajima, O. Morimoto, Sh. Xu, Y. Moritomo, N. Hamada, Y. Aiura, *Phys. Rev. B* **72**, 045107 (2005).
 - ¹⁵ K.-I. Kobayashi, T. Kimura, H. Sawada, K. Terakura, and Y. Tokura, *Nature (London)* **395**, 677 (1998).
 - ¹⁶ D.D. Sarma, *Current Opinion in Solid State and Materials Science*, **5**, 261 (2001).
 - ¹⁷ J. B. Philipp, P. Majewski, L. Alff, A. Erb, R. Gross, T. Graf, M. S. Brandt, J. Simon, T. Walther, W. Mader, D. Topwal, and D. D. Sarma, *Phys. Rev. B*, **68**, 144431 (2003); H. Kato, T. Okuda, Y. Okimoto, Y. Tomioka, Y. Takenoya, A. Ohkubo, M. Kawasaki, and Y. Tokura, *App. Phys. Lett* **81**, 328 (2002); Y. Krockenberger, K. Mogare, M. Reehuis, M. Tovar, M. Jansen, G. Vaitheeswaran, V. Kanchana, F. Bultmark, A. Delin, F. Wilhelm, A. Rogalev, A. Winkler, and L. Alff, *Phys. Rev. B* **75**, 020404 (2007).
 - ¹⁸ F. K. Patterson, C. W. Moeller, and R. Ward, *Inorg. Chem.* **2**, 196 (1963).
 - ¹⁹ A. Arulraj, K. Ramesha, J. Gopalakrishnan, and C. N. R. Rao, *J. Solid State Chem.* **155**, 233 (2000).
 - ²⁰ Y. Moritomo, Sh Xu, A. Machida, T. Akimoto, E. Nishibori, M. Takata and M. Sakata, *Phys. Rev. B* **61**, R7827 (2000).
 - ²¹ T.S. Chana, R.S. Liua, G.Y. Guoc, S.F. Hud, J.G. Line, J.-F. Leef, L.-Y. Jangf, C.-R. Changb, C.Y. Huangg, *Solid State Commun.* **131**, 531 (2004).
 - ²² C.M. Bonilla, D.A. Landnez Tellez, J. Arbey Rodrguez, E. Vera Lopez, J. Roa-Rojas, *Physica B* **398**, 208 (2007).
 - ²³ H. Wu, *Phys. Rev. B* **64**, 125126 (2001).
 - ²⁴ G. Dimitri Ngantso, A. Benyoussef, A. El Kenz, S. Naji, *J Supercond Nov Magn* **28**, 2589 (2015).
 - ²⁵ G. Kresse and J. Hafner, *Phys. Rev. B* **47**, R558 (1993), G. Kresse and J. Furthmuller, *Phys. Rev. B* **54**, 11169 (1996).
 - ²⁶ John P. Perdew, J. A. Chevary, S. H. Vosko, Koblar A. Jackson, Mark R. Pederson, D. J. Singh, and Carlos Fiolhais, *Phys. Rev. B* **46**, 6671 (1992).
 - ²⁷ W. Kohn and L. J. Sham *Phys. Rev.* **140**, A1133 (1965); R.

- G. Parr and W. Yang Density Functional Theory of Atoms and Molecules Oxford University Press, Oxford (1989).
- ²⁸ J. P. Perdew, K. Burke, and M. Ernzerhof, Phys. Rev. Lett. **77**, 3865 (1996).
- ²⁹ P. E. Blöchl, Phys. Rev. B **50**, 17953 (1994).
- ³⁰ O. K. Andersen and T. Saha-Dasgupta, Phys. Rev. B **62**, R16219 (2000).
- ³¹ O. K. Andersen, Phys. Rev. B **12**, 3060 (1975).
- ³² J. Kunes, R. Arita, P. Wissgott, A. Toschi, H. Ikeda, and K. Held, Comp. Phys. Comm. **181**, 1888 (2010).
- ³³ A. A. Mostofi, J. R. Yates, Y.-S. Lee, I. Souza, D. Vanderbilt and N. Marzari Comput. Phys. Commun. **178**, 685 (2008).
- ³⁴ S. P. Blaha, K. Schwartz, G. K. H. Madsen, D. Kvasnicka & J. Luitz. WIEN2K, An Augmented Plane Wave+ Local Orbitals Program for Calculating Crystal Properties. edited by K. Schwarz . Technische Universitaet Wien, Austria (2001).
- ³⁵ G. Kotliar, S. Y. Savrasov, K. Haule, V. S. Oudovenko, O. Parcollet, and C. A. Marianetti, Rev. Mod. Phys. **78**, 865 (2006).
- ³⁶ K. Held, Advances in Physics **56**, 829 (2007).
- ³⁷ N. Parragh, A. Toschi, K. Held, and G. Sangiovanni, Phys. Rev. B **86**, 155158 (2012); M. Wallerberger (unpublished).
- ³⁸ C. Taranto, M. Kaltak, N. Parragh, G. Sangiovanni, G. Kresse, A. Toschi, and K. Held, Phys. Rev. B **88**, 165119 (2013).
- ³⁹ L. Si, Z. Zhong, J. M. Tomczak, and K. Held Phys. Rev. B **92**, 041108(R) (2015).
- ⁴⁰ E. Gull, A. J. Mills, A. I. Lichtenstein, A. N. Rubtsov, M. Troyer, P. Werner, Rev. Mod. Phys. **83**, 349 (2011).
- ⁴¹ Q. F. Li, X. F. Zhu and L. F. Chen, J. Phys.: Condens. Matter **20**, 255230 (2008)
- ⁴² Prabuddha Sanyal, Hena Das, and T. Saha-Dasgupta, Phys. Rev. B **80**, 224412 (2009).
- ⁴³ Hena Das, Prabuddha Sanyal, T. Saha-Dasgupta and D.D. Sarma, Phys. Rev. B, **83**, 104418 (2011).
- ⁴⁴ J. Blasco, C. Ritter, L. Morellón, P. A. Algarabel, J. M. De Teresa, D. Serrate, J. García and R. M. Ibarra, Solid State Sci. **4**, 651 (2002).
- ⁴⁵ The sharp spikes in the Cr- t_{2g} up spin channel above the Fermi level might well be an artefact of the maximum entropy method employed for the analytical continuation.
- ⁴⁶ J. Kanamori and K. Terakura, J. Phys. Soc. Jpn. **70**, 1433 (2001).
- ⁴⁷ K. Samanta, P. Sanyal and T. Saha-Dasgupta, Scientific Reports **5**, 15010 (2015).
- ⁴⁸ H. Iwasawa, K. Yamakawa, T. Saitoh, J. Inaba, T. Katsufuji, M. Higashiguchi, K. Shimada, H. Namatame, M. Taniguchi, Phys. Rev. Lett **96**, 067203 (2006); H. Iwasawa, S. Kaneyoshi, K. Kurahashi, T. Saitoh, I. Hase, T. Katsufuji, K. Shimada, H. Namatame, and M. Taniguchi, Phys. Rev. B **80**, 125122 (2009).
- ⁴⁹ We have also repeated the NMTO calculation to obtain the energy level diagram and intrinsic spin splitting at the B' site, by carrying out calculations of SCWO with same crystal structure as SCMO, constructed by replacing Mo by W in the SCMO lattice. Comparison of the intrinsic spin-splitting observed at Mo site in case of SCMO as compared to that at W site of this hypothetical SCWO compound, captures solely the chemical effect, eliminating any possible lattice effect. The obtained result shows the intrinsic spin splitting at the W site of the hypothetical SCWO compound to be 0.05 eV, in good agreement with the value of 0.06 eV obtained for the SCWO⁴³ in its own crystal structure. This proves the dominance of chemical effect (W versus Mo) compared to the lattice effect.
- ⁵⁰ O. Navarro, E. Carvajal, B. Aguilar, M. Avignon, Physica B **384**, 110 (2006); L. Brey, M. J. Calderón, S. Das Sarma and F. Guinea, Phys. Rev. B **74**, 094429 (2006); J.L.Alonso,L.A. Fernandez, F. Guinea, F. Lesmes, and V. Martin-Mayor, Phys. Rev. B, **67**, 214423 (2003).
- ⁵¹ The energy difference between PM and FM phases for different lattice sizes are found to scale with size, although the ratio between values for SCMO and SCWO is found to remain almost the same in calculations on different lattice sizes. These values are found to be 0.050 eV/f.u. for SCMO, 0.063 eV/f.u. for SCWO with a ratio of 79.2 % for a 4x4x4 lattice, 0.066 eV/f.u. for SCMO, 0.084 eV/f.u. for SCWO with a ratio of 78.5 % for a 6x6x6 lattice, and 0.067 eV/f.u. for SCMO, 0.085 eV/f.u. for SCWO with a ratio of 78.8 % for a 8x8x8 lattice. The values presented in the text are for 8x8x8.